BDDC PRECONDITIONERS FOR SPECTRAL ELEMENT DISCRETIZATIONS OF ALMOST INCOMPRESSIBLE ELASTICITY IN THREE DIMENSIONS[*]

LUCA F. PAVARINO[†], OLOF B. WIDLUND[‡], AND STEFANO ZAMPINI[§]

Abstract. Balancing domain decomposition by constraints (BDDC) algorithms are constructed and analyzed for the system of almost incompressible elasticity discretized with Gauss–Lobatto–Legendre spectral elements in three dimensions. Initially mixed spectral elements are employed to discretize the almost incompressible elasticity system, but a positive definite reformulation is obtained by eliminating all pressure degrees of freedom interior to each subdomain into which the spectral elements have been grouped. Appropriate sets of primal constraints can be associated with the subdomain vertices, edges, and faces so that the resulting BDDC methods have a fast convergence rate independent of the almost incompressibility of the material. In particular, the condition number of the BDDC preconditioned operator is shown to depend only weakly on the polynomial degree n, the ratio H/h of subdomain and element diameters, and the inverse of the inf-sup constants of the subdomains and the underlying mixed formulation, while being scalable, i.e., independent of the number of subdomains and robust, i.e., independent of the Poisson ratio and Young's modulus of the material considered. These results also apply to the related dual-primal finite element tearing and interconnect (FETI-DP) algorithms defined by the same set of primal constraints. Numerical experiments, carried out on parallel computing systems, confirm these results.

Key words. domain decomposition, balancing domain decomposition by constraints preconditioners, almost incompressible elasticity, mixed spectral elements

AMS subject classifications. 65F08, 65N30, 65N35, 65N55

DOI. 10.1137/100791701

1. Introduction. The purpose of this paper is to construct and analyze balancing domain decomposition by constraints (BDDC) algorithms, (see [13, 41]) for the system of almost incompressible elasticity in three dimensions, discretized with Gauss–Lobatto–Legendre (GLL) spectral elements. As the material becomes almost incompressible, the resulting discrete system becomes extremely ill conditioned, particularly so when increasing the polynomial degree of the spectral elements. Therefore, it is quite a challenge to devise domain decomposition preconditioners that maintain scalability and fast convergence rates also for almost incompressible materials. Our algorithm builds on earlier work by Li and Widlund [36] for the Stokes system, but here we can work with a positive definite reformulation of an underlying mixed formulation of the elasticity system, obtained by eliminating all displacement and pressure degrees of freedom interior to each subdomain into which the spectral elements have been grouped. Our overall strategy assumes that the set of primal constraints works well in the compressible case and, in addition, that a no net flux condition is satisfied across the boundary of each subdomain. We show that appropriate sets of primal

constraints can be associated with the subdomain vertices, edges, and faces so that the resulting BDDC methods have a fast convergence rate independent of the material being almost incompressible. In particular, we prove that the condition number of the BDDC preconditioned operator depends only weakly on the polynomial degree n, the ratio H/h of subdomain to element diameters, and the inverse of the inf-sup constants of the subdomains and the underlying mixed formulation, while being independent of the number of subdomains (scalability) and of the Poisson ratio and Young's modulus of the material considered (robustness). The results of numerical experiments on parallel computing systems confirm our theory and illustrate the effects of the choice of the primal constraints. A preliminary study in two dimensions and without proofs can be found in [47]. We are currently working on the extension of inexact BDDC algorithms (see, e.g., [15, 38]) to GLL spectral elements and almost incompressible elasticity. We remark that our results also apply to the related dual-primal finite element tearing and interconnect (FETI-DP) algorithms (see, e.g., [19, 33]) defined by the same set of primal constraints, since it is known that the BDDC and FETI-DP operators have the same eigenvalues with the exception of at most two; see [41, 37, 7].

BDDC methods can be regarded as an evolution of balancing Neumann–Neumann methods where all local and coarse problems are treated additively and a proper set of *primal continuity constraints* across the interface of the subdomains is selected, just as in FETI-DP methods. These primal constraints can be point constraints and averages and moments over edges and/or faces of the subdomains. Several choices will be considered in sections 6 and 8.

Earlier works on domain decomposition algorithms for mixed elasticity and Stokes systems have focused on wirebasket and balancing Neumann–Neumann methods [45, 46, 22], [5], on FETI-DP and BDDC methods for the incompressible limit [14], [35, 36], [32], and on overlapping Schwarz and hybrid methods [26, 16, 17]. Previous works on BDDC and FETI-DP algorithms for GLL spectral elements have focused on the scalar elliptic case only; see [44, 27]. The BDDC algorithm has been extended to a variety of cases, including mortar discretizations [23, 24, 25], discontinuous Galerkin methods [18], Stokes–Darcy coupling [20], advection-diffusion and indefinite problems [51, 39], inexact solvers [15, 38], Reissner–Mindlin plates [4], and multilevel algorithms [49, 50, 43]; see also [42]. We refer to the monograph by Toselli and Widlund [48] for an introduction to domain decomposition methods and to those by Deville, Fischer, and Mund [11] and by Canuto et al. [9] for introductions to spectral element methods. In comparison with previous domain decomposition methods for Stokes and mixed elasticity, such as wirebasket [45], balancing Neumann–Neumann [46, 22, 5], and overlapping Schwarz [26] methods, BDDC represents very significant progress, yielding much smaller condition numbers and being easier to implement than previous iterative substructuring methods. We also note that FETI-DP and BDDC algorithms have proven very important in computational elasticity.

The rest of the paper is organized as follows. In section 2, we introduce the almost incompressible elasticity system, discretize it with a mixed spectral element method based on GLL quadrature, and reformulate it as a positive definite system by eliminating all pressure variables; this is followed by eliminating the displacements interior to each subdomain. The resulting interface problem and interface space are further decomposed in section 3, where we also define the required restriction and interpolation operators, Schur complements, and certain interface norms. We also formulate a lemma which highlights the importance of a no net flux condition. The BDDC preconditioner is introduced in section 4. The main BDDC convergence rate estimate and auxiliary results are presented in section 5. Several choices of sets of

primal constraints are considered in section 6 and associated transformations of basis functions in section 7. The paper concludes by section 8 with the results of several numerical experiments in three dimensions on parallel computer systems.

2. Almost incompressible elasticity and spectral elements.

2.1. The continuous problem. We consider a domain $\Omega \subset R^3$, decomposed into N nonoverlapping subdomains Ω_i of diameter H_i, and forming a coarse finite element partition of Ω,

$$\overline{\Omega} = \bigcup_{i=1}^{N} \overline{\Omega}_i. \tag{2.1}$$

Let $H = \max_i H_i$ be the characteristic diameter of the subdomains and $\partial\Omega_D$ a nonempty subset of $\partial\Omega$. We consider a mixed formulation of linear elasticity for almost incompressible materials as, e.g., in [8]: find $(\mathbf{u}, p) \in \mathbf{V} \times U$ such that

$$\begin{cases} 2 \int_{\Omega} \mu\epsilon(\mathbf{u}) : \epsilon(\mathbf{v}) \ dx - \int_{\Omega} \text{div } \boldsymbol{v} \ p \ dx = \langle \mathbf{F}, \mathbf{v} \rangle & \forall \mathbf{v} \in \mathbf{V}, \\ \\ -\int_{\Omega} \text{div } \boldsymbol{u} \ q \ dx - \int_{\Omega} 1/\lambda pq \ dx = 0 & \forall q \in U. \end{cases} \tag{2.2}$$

The functional spaces are

$$\mathbf{V} := \{\mathbf{v} \in H^1(\Omega)^3 : \mathbf{v}|_{\partial\Omega_D} = 0\}, \qquad U := L^2(\Omega) \ \text{ (or } L_0^2(\Omega) \text{ if } \partial\Omega_D = \partial\Omega).$$

$\mathbf{F}$ represents the applied forces, and $\mu(x)$ and $\lambda(x)$ are the Lamé parameters of the material that, for simplicity, we assume constant in each subdomain Ω_i; they can be expressed in terms of the local Poisson ratio ν_i and Young's modulus E_i as

$$\mu_i := \frac{E_i}{2(1+\nu_i)}, \qquad \lambda_i := \frac{E_i\nu_i}{(1+\nu_i)(1-2\nu_i)}. \tag{2.3}$$

The material of a subdomain approaches the incompressible limit when $\nu_i \to 1/2$. Factoring out the constants μ_i and $\frac{1}{\lambda_i}$, we can define local bilinear forms by

$$\sum_{i=1}^{N} \mu_i a_i(\mathbf{u}, \mathbf{v}) := 2 \sum_{i=1}^{N} \mu_i \int_{\Omega_i} \varepsilon(\mathbf{u}) : \varepsilon(\mathbf{v}) \ dx, \quad \sum_{i=1}^{N} \frac{1}{\lambda_i} c_i(p, q) := \sum_{i=1}^{N} \frac{1}{\lambda_i} \int_{\Omega_i} p \ q \ dx, \tag{2.4}$$

and also by

$$\sum_{i=1}^{N} b_i(\mathbf{v}, q) := -\sum_{i=1}^{N} \int_{\Omega_i} \text{div}\mathbf{v} \ q \ dx. \tag{2.5}$$

The global problem (2.2) is obtained by assembling contributions to the bilinear forms from the different subdomains. Our convergence rate analysis will be reduced to developing bounds for individual subdomains. The resulting estimates will be independent of the values of the Lamé parameters.

2.2. Mixed GLL spectral elements. Let T_{ref} be the reference cube $(-1,1)^3$, and let $Q_n(T_{\text{ref}})$ be the set of polynomials on T_{ref} of degree $n \geq 1$ in each variable. We

assume that the domain Ω can be decomposed into N_e nonoverlapping finite elements T_k of diameter h_k,

$$(2.6) \qquad \overline{\Omega} = \bigcup_{k=1}^{N_e} \overline{T}_k,$$

each of which is an affine image of the reference cube, i.e., $T_k = \phi_k(T_{\text{ref}})$, where ϕ_k is an affine mapping. This is a standard assumption in the spectral element literature, and our proof will rely on it. At present, we do not have a proof for spectral element discretizations with more general mappings (see, e.g., [21] for a numerical study of overlapping Schwarz preconditioners for spectral elements based on transfinite mappings). Let $h = \max_k h_k$ be the characteristic diameter of the elements. We assume that this finite element partition, (2.6), is a refinement of the coarse subdomain partition $\{\Omega_i\}_{i=1}^{N}$ defined previously in (2.1), with finite element nodes matching across the interfaces between neighboring subdomains. Hence each $\overline{\Omega}_i$ is the union of a subset of the closure of elements T_k.

The space of displacements $\mathbf{V}$ is discretized, component by component, by continuous, piecewise tensor product polynomials of degree n:

$$\mathbf{V}_n := \left\{ \mathbf{v} \in \mathbf{V} : v_k|_{T_i} \circ \phi_i \in Q_n(T_{\text{ref}}), \ i = 1, 2, \ldots, N_e, \ k = 1, 2, 3 \right\}.$$

The pressure space U is discretized by discontinuous, piecewise tensor product polynomials of degree $n - 2$:

$$U_n := \left\{ q \in U : q|_{T_i} \circ \phi_i \in Q_{n-2}(T_{\text{ref}}), \ i = 1, 2, \ldots, N_e \right\}.$$

We use GLL(n) quadrature, which also allows for the construction of very convenient nodal tensor-product bases for $\mathbf{V}_n$ and U_n, using for the latter only the interior GLL nodes of each element. We denote by $\{\xi_i\}_{i=0}^{n}$ the set of GLL(n) points of $[-1, 1]$, by σ_i the quadrature weight associated with ξ_i, and by $l_i(x)$ the Lagrange interpolating polynomial of degree n that vanishes at all the GLL(n) nodes except at ξ_i, where it equals 1. Each element of $Q_n(T_{\text{ref}})$ is expanded in this GLL(n) basis, and any L^2–inner product of two scalar components u and v is replaced by

$$(2.7) \qquad (u,v)_{n,\Omega} = \sum_{s=1}^{N_e} \sum_{i,j,k=0}^{n} (u \circ \phi_s)(\xi_i, \xi_j, \xi_k)(v \circ \phi_s)(\xi_i, \xi_j, \xi_k)|J_s|\sigma_i \sigma_j \sigma_k \,,$$

where $|J_s|$ is the determinant of the Jacobian of ϕ_s. Similarly, a very convenient basis for U_n consists of the tensor-product Lagrangian nodal basis functions associated with the internal GLL(n) nodes; i.e., the endpoints -1 and $+1$ are excluded. The mass matrix based on these basis elements and GLL(n) quadrature is then diagonal for the displacement field but not for the pressure field.

The $Q_n - Q_{n-2}$ method satisfies a nonuniform inf-sup condition

$$(2.8) \qquad \sup_{\mathbf{v} \in \mathbf{V}_n} \frac{(\text{div}\mathbf{v}, q)}{\|\mathbf{v}\|_{H^1}} \geq \beta_n \|q\|_{L^2} \quad \forall q \in U_n \,,$$

where $\beta_n \geq Cn^{-1}$ and the constant $C > 0$ is independent of n. It is also known that β_n decays slower for small n than indicated by the theoretical bound; for example, $\beta_n \geq 0.43$ for $n \leq 16$ according to Maday et al. [40]. (We note, however, that the inf-sup coefficient will decrease with an increase in the aspect ratio of a domain; see Dobrowolski [12].) An alternative mixed spectral element method, with a bound on the inf-sup constant which does not depend on n, is provided by the $Q_n - P_{n-1}$ method; see Bernardi and Maday [6].

2.3. The discrete system and its positive definite reformulation. The discrete system, obtained from the GLL spectral elements, is assembled from the saddle point matrices of individual subdomains Ω_i:

$$\left[\begin{array}{cc} \mu_i A^{(i)} & B^{(i)T} \\ B^{(i)} & -1/\lambda_i \ C^{(i)} \end{array} \right],$$

where $\mu_i A^{(i)}, B^{(i)}$, and $1/\lambda_i \ C^{(i)}$ are the local matrices associated with the local components of the bilinear forms as in (2.4), (2.5).

Since we are using discontinuous pressures, all pressure degrees of freedom can be eliminated, element by element, to obtain reduced positive definite stiffness matrices

(2.9) $$K^{(i)} := \mu_i A^{(i)} + \lambda_i B^{(i)T} C^{(i)-1} B^{(i)}$$

that can be subassembled into a global positive definite stiffness matrix K.

The load vector of the full system can similarly be assembled from contributions from the elements.

3. Subspace decomposition and operators. We recall that the computational domain $\Omega \subset R^3$ has been decomposed in (2.1) into N nonoverlapping subdomains Ω_i of characteristic size H. In our experiments, they each consist of $(H/h)^3$ spectral elements T_k of characteristic size h, while in our theory, we can allow less regular subdomains. The subdomain interface is designated by $\Gamma := \bigcup_{i \neq j} \partial\Omega_i \cap \partial\Omega_j$. We assume matching finite element nodes on the boundaries of adjacent subdomains across the interface.

We split the set of basis functions into interior functions with the subscript I and the remaining interface basis functions with the subscript Γ.

3.1. Subspaces. We will use the framework of [37]. Let $\boldsymbol{V}^{(i)}$ be the local space of spectral element displacements defined on Ω_i and that vanish on $\partial\Omega_i \cap \partial\Omega_D$. We split this space into a direct sum of its interior and interface subspaces $\boldsymbol{V}^{(i)} = \boldsymbol{V}_I^{(i)} \bigoplus \boldsymbol{V}_\Gamma^{(i)}$, and we define the associated product spaces by

$$\boldsymbol{V}_I := \prod_{i=1}^{N} \boldsymbol{V}_I^{(i)}, \quad \boldsymbol{V}_\Gamma := \prod_{i=1}^{N} \boldsymbol{V}_\Gamma^{(i)}.$$

The functions in $\boldsymbol{V}_\Gamma$ are generally discontinuous across Γ, while our spectral element approximations of the displacements are not. Therefore, we also define the subspace

$$\widehat{\boldsymbol{V}}_\Gamma := \{\text{functions of } \boldsymbol{V}_\Gamma \text{ that are continuous across } \Gamma\}.$$

We will also need an intermediate subspace $\widetilde{\boldsymbol{V}}_\Gamma$ defined by further splitting the interface degrees of freedom into primal (with the subscript Π) and dual (with the subscript Δ) degrees of freedom:

$$\widetilde{\boldsymbol{V}}_\Gamma := \boldsymbol{V}_\Delta \bigoplus \widehat{\boldsymbol{V}}_\Pi.$$

Here

(a) $\widehat{\boldsymbol{V}}_\Pi$ is a global subspace consisting of selected continuous functions, the *primal* variables; these can be the subdomain vertex basis functions of $\widehat{\boldsymbol{V}}$ and/or edge/face basis functions with a constant value at the nodes of the associated edge/face. We will assume that, after a change of basis, each primal variable corresponds to an

explicit degree of freedom; cf. [37, section 3.3] and subsection 7. This simplifies the presentation and also adds to the robustness of the algorithms; see [28, 29].

(b) $\boldsymbol{V}_\Delta = \prod_{i=1}^N \boldsymbol{V}_\Delta^{(i)}$ is the product space of the subspaces $\boldsymbol{V}_\Delta^{(i)}$ of *dual* interface functions that vanish at the primal degrees of freedom.

3.2. Restriction and scaling operators. In order to define our preconditioners, we need certain restriction and interpolation operators represented by matrices with elements in the set $\{0, 1\}$:

$$(3.1) \qquad \begin{array}{llll} R_{\Gamma\Delta} : \widetilde{\boldsymbol{V}}_\Gamma \longrightarrow \boldsymbol{V}_\Delta, & R_{\Gamma\Pi} : \widetilde{\boldsymbol{V}}_\Gamma \longrightarrow \widehat{\boldsymbol{V}}_\Pi, & \overline{R}_\Gamma : \widetilde{\mathbf{V}}_\Gamma \longrightarrow \mathbf{V}_\Gamma, \\ R_\Gamma^{(i)} : \widehat{\boldsymbol{V}}_\Gamma \longrightarrow \boldsymbol{V}_\Gamma^{(i)}, & R_\Delta^{(i)} : \boldsymbol{V}_\Delta \longrightarrow \boldsymbol{V}_\Delta^{(i)}, & R_\Pi^{(i)} : \widehat{\boldsymbol{V}}_\Pi \longrightarrow \boldsymbol{V}_\Pi^{(i)}. \end{array}$$

With these operators, we build the following operators:

$$R_\Gamma : \widehat{\boldsymbol{V}}_\Gamma \longrightarrow \boldsymbol{V}_\Gamma, \text{ the direct sum of the } R_\Gamma^{(i)},$$

$$\widetilde{R}_\Gamma : \widehat{\boldsymbol{V}}_\Gamma \longrightarrow \widetilde{\boldsymbol{V}}_\Gamma, \text{ the direct sum } R_{\Gamma\Pi} \oplus R_\Delta^{(i)} R_{\Gamma\Delta}.$$

We will also need the standard counting functions of the Neumann–Neumann methods and in particular their pseudoinverses $\delta_i^\dagger(x)$, defined at each node x on the interface $\Gamma_i := \partial\Gamma_i \cap \Gamma$ of subdomain Ω_i by

$$(3.2) \qquad \delta_i^\dagger(x) := \mu_i(x)/\left(\sum_{j \in \mathcal{N}_x} \mu_j(x)\right),$$

where μ_i is the value of the first Lamé parameter on Ω_i and $\mathcal{N}_x$ is the set of indices of the subdomains having the node x on their boundaries; see also [48, section 6.2.1] for alternatives. We define scaled local restriction operators $R_{D,\Gamma}^{(i)}$ and $R_{D,\Delta}^{(i)}$ by multiplying the sole nonzero element of each row of $R_\Gamma^{(i)}$ and $R_\Delta^{(i)}$ by $\delta_i^\dagger(x)$. Then let

$$R_{D,\Gamma} := \text{ the direct sum of } R_{D,\Gamma}^{(i)}, \quad \widetilde{R}_{D,\Gamma} := \text{ the direct sum } R_{\Gamma\Pi} \oplus R_{D,\Delta}^{(i)} R_{\Gamma\Delta}.$$

3.3. Schur complements. After reordering the interior displacements first and then those of the interface into $(\mathbf{u}_I, \mathbf{u}_\Gamma)$, the local spectral element stiffness matrix for subdomain Ω_i can be rewritten as

$$K^{(i)} := \left[\begin{array}{cc} K_{II}^{(i)} & K_{\Gamma I}^{(i)T} \\ K_{\Gamma I}^{(i)} & K_{\Gamma\Gamma}^{(i)} \end{array} \right].$$

By eliminating the interior displacement variables, we obtain the local Schur complement $S_\Gamma^{(i)}$, of the subdomain Ω_i, as

$$S_\Gamma^{(i)} := K_{\Gamma\Gamma}^{(i)} - K_{\Gamma I}^{(i)} K_{II}^{(i)-1} K_{\Gamma I}^{(i)T}.$$

We note that while the pressures have been explicitly eliminated in (2.9) in order to obtain a positive definite reformulation, the interior displacements are only eliminated implicitly. Indeed, as is standard practice in iterative substructuring methods, only the actions of $S_\Gamma^{(i)}$ on given vectors will be required by the preconditioned conjugate gradient (PCG) method employed, and these actions will be computed by solving local Dirichlet problems on each Ω_i. The BDDC preconditioner will also require the

solution of additional local problems with natural boundary conditions except with vanishing primal displacement components.

We will consider three Schur complements corresponding to the spaces $\mathbf{V}_\Gamma, \widehat{\mathbf{V}}_\Gamma$, and $\widetilde{\mathbf{V}}_\Gamma$: (a) the Schur complement S_Γ defined on the space $\mathbf{V}_\Gamma$ as the direct sum of the local Schur complements $S_\Gamma^{(i)}$:

$$(3.3) \qquad S_\Gamma := \begin{bmatrix} S_\Gamma^{(1)} & 0 & \cdots & 0 \\ 0 & S_\Gamma^{(2)} & & \vdots \\ \vdots & & \ddots & 0 \\ 0 & \cdots & 0 & S_\Gamma^{(N)} \end{bmatrix}.$$

By subassembling all the degrees of freedom of the local Schur complements, we obtain (b) the classical Schur complement $\widehat{S}_\Gamma$, defined on the continuous subspace $\widehat{\mathbf{V}}_\Gamma$:

$$\widehat{S}_\Gamma := \sum_{i=1}^{N} R_\Gamma^{(i)T} S_\Gamma^{(i)} R_\Gamma^{(i)} = R_\Gamma^T S_\Gamma R_\Gamma,$$

with S_Γ defined in (3.3).

And finally, (c) the intermediate Schur complement $\widetilde{S}_\Gamma$, defined over the partially assembled interface space $\widetilde{\mathbf{V}}_\Gamma$, obtained by assembling only the primal variables of the $S_\Gamma^{(i)}$:

$$\widetilde{S}_\Gamma := \overline{R}_\Gamma^T S_\Gamma \overline{R}_\Gamma,$$

with $\overline{R}_\Gamma : \widetilde{\mathbf{V}}_\Gamma \longrightarrow \mathbf{V}_\Gamma$ defined in (3.1) and S_Γ in (3.3). The classical Schur complement $\widehat{S}_\Gamma$ can be also obtained from $\widetilde{S}_\Gamma$ by further assembling the dual variables, i.e., as

$$(3.4) \qquad \widehat{S}_\Gamma := \widetilde{R}_\Gamma^T \widetilde{S}_\Gamma \widetilde{R}_\Gamma.$$

3.4. Interface norms and seminorms. We define the following $S_\Gamma^{(i)}$- and S_Γ-seminorms by

$$(3.5) \qquad |\mathbf{w}_\Gamma^{(i)}|_{S_\Gamma^{(i)}}^2 := \mathbf{w}_\Gamma^{(i)T} S_\Gamma^{(i)} \mathbf{w}_\Gamma^{(i)} \quad \forall \mathbf{w}_\Gamma^{(i)} \in \mathbf{V}_\Gamma^{(i)},$$

$$(3.6) \qquad |\mathbf{w}_\Gamma|_{S_\Gamma}^2 := \mathbf{w}_\Gamma^T S_\Gamma \mathbf{w}_\Gamma = \sum_{i=1}^{N} |\mathbf{w}_\Gamma^{(i)}|_{S_\Gamma^{(i)}}^2 \quad \forall \mathbf{w}_\Gamma \in \mathbf{V}_\Gamma,$$

the $\widehat{S}_\Gamma$- and $\widetilde{S}_\Gamma$-norms by

$$(3.7) \qquad \|\mathbf{w}_\Gamma\|_{\widehat{S}_\Gamma}^2 := \mathbf{w}_\Gamma^T R_\Gamma^T S_\Gamma R_\Gamma \mathbf{w}_\Gamma = |R_\Gamma \mathbf{w}_\Gamma|_{S_\Gamma}^2 \quad \forall \mathbf{w}_\Gamma \in \widehat{\mathbf{V}}_\Gamma,$$

$$(3.8) \qquad \|\mathbf{w}_\Gamma\|_{\widetilde{S}_\Gamma}^2 := \mathbf{w}_\Gamma^T \overline{R}_\Gamma^T S_\Gamma \overline{R}_\Gamma \mathbf{w}_\Gamma = |\overline{R}_\Gamma \mathbf{w}_\Gamma|_{S_\Gamma}^2 \quad \forall \mathbf{w}_\Gamma \in \widetilde{\mathbf{V}}_\Gamma,$$

and the $|\cdot|_{E(\Gamma_i)}$- and $|\cdot|_{E(\Gamma)}$-seminorms by

$$(3.9) \qquad |\mathbf{w}_\Gamma^{(i)}|_{E(\Gamma_i)} := \inf_{\substack{\mathbf{v}^{(i)} \in \mathbf{V}^{(i)} \\ \mathbf{v}^{(i)}|_{\Gamma_i} = \mathbf{w}_\Gamma^{(i)}}} \|\epsilon(\mathbf{v}^{(i)})\|_{L^2(\Omega_i)},$$

$$(3.10) \qquad |\mathbf{w}_\Gamma|_{E(\Gamma)}^2 := \sum_{i=1}^{N} \mu_i |\mathbf{w}_\Gamma^{(i)}|_{E(\Gamma_i)}^2 \quad \forall \mathbf{w}_\Gamma \in \mathbf{V}_\Gamma.$$

We note that the $|\cdot|_{E(\Gamma_i)}$-seminorm can also be written in terms of the local stiffness matrix $A^{(i)}$ since $\|\epsilon(\mathbf{v}^{(i)})\|_{L^2(\Omega_i)}^2 = \mathbf{v}^{(i)T} A^{(i)} \mathbf{v}^{(i)}$.

The following lemma, which is a consequence of Lemma 3.3 in Dohrmann and Widlund [17], will allow us to reduce our analysis in section 5 from the almost incompressible to the compressible case.

LEMMA 3.1. *If $\mathbf{w}_\Gamma^{(i)}$ has zero net flux across a subdomain boundary, i.e.,*

$$\int_{\partial\Omega_i} (\mathbf{w}_\Gamma^{(i)}) \cdot \mathbf{n}_i dA = 0,$$

with $\mathbf{n}_i$ the unit outward normal to the subdomain boundary and $\beta_{n,i}$ the inf-sup parameter of Ω_i, then

$$\mu_i |\mathbf{w}_\Gamma^{(i)}|_{E(\Gamma_i)}^2 \le |\mathbf{w}_\Gamma^{(i)}|_{S_\Gamma^{(i)}}^2 \le 4 \left(1 + \frac{3/2}{\mu_i/\lambda_i + \beta_{n,i}^2} \right) \mu_i |\mathbf{w}_\Gamma^{(i)}|_{E(\Gamma_i)}^2.$$

4. The BDDC preconditioner. The splitting of the interface displacements into dual (with subscript Δ) and primal (with subscript Π) interface displacements induces the following partition of the local stiffness matrices:

$$K^{(i)} := \left[\begin{array}{ccc} K_{II}^{(i)} & K_{\Delta I}^{(i)T} & K_{\Pi I}^{(i)} \\ K_{\Delta I}^{(i)} & K_{\Delta\Delta}^{(i)} & K_{\Pi\Delta}^{(i)T} \\ K_{\Pi I}^{(i)} & K_{\Pi\Delta}^{(i)} & K_{\Pi\Pi}^{(i)} \end{array} \right].$$

The BDDC preconditioner for the Schur complement $\widehat{S}_\Gamma$ is defined by

$$(4.1) \qquad\qquad\qquad M^{-1} := \widetilde{R}_{D,\Gamma}^T \widetilde{S}_\Gamma^{-1} \widetilde{R}_{D,\Gamma},$$

where
(4.2)

$$\widetilde{S}_\Gamma^{-1} := R_{\Gamma\Delta}^T \left(\sum_{i=1}^N \left[\begin{array}{cc} 0 & R_\Delta^{(i)T} \end{array} \right] \left[\begin{array}{cc} K_{II}^{(i)} & K_{\Delta I}^{(i)T} \\ K_{\Delta I}^{(i)} & K_{\Delta\Delta}^{(i)} \end{array} \right]^{-1} \left[\begin{array}{c} 0 \\ R_\Delta^{(i)} \end{array} \right] \right) R_{\Gamma\Delta} + \Phi S_{\Pi\Pi}^{-1} \Phi^T.$$

This formula can be obtained by a block-Cholesky factorization of a partially subassembled problem; see [37]. The first term in (4.2) represents local Neumann solves on individual subdomain Ω_i with the primal variables constrained to vanish. The second term involves a coarse, global solve for the primal variables, with the coarse matrix

$$S_{\Pi\Pi} = \sum_{i=1}^N R_\Pi^{(i)T} \left(K_{\Pi\Pi}^{(i)} - \left[\begin{array}{cc} K_{\Pi I}^{(i)} & K_{\Pi\Delta}^{(i)} \end{array} \right] \left[\begin{array}{cc} K_{II}^{(i)} & K_{\Delta I}^{(i)T} \\ K_{\Delta I}^{(i)} & K_{\Delta\Delta}^{(i)} \end{array} \right]^{-1} \left[\begin{array}{c} K_{\Pi I}^{(i)T} \\ K_{\Pi\Delta}^{(i)T} \end{array} \right] \right) R_\Pi^{(i)}$$

and a matrix Φ representing a change from discontinuous interface variables to primal degree of freedoms. It is formed by the coarse basis functions defined on $\widetilde{V}_\Gamma$ and as the minimum energy extension into the subdomains, subject to the set of primal constraints, and is given by

$$\Phi = R_{\Gamma\Pi}^T - R_{\Gamma\Delta}^T \sum_{i=1}^N \left[\begin{array}{cc} 0 & R_\Delta^{(i)T} \end{array} \right] \left[\begin{array}{cc} K_{II}^{(i)} & K_{\Delta I}^{(i)T} \\ K_{\Delta I}^{(i)} & K_{\Delta\Delta}^{(i)} \end{array} \right]^{-1} \left[\begin{array}{c} K_{\Pi I}^{(i)T} \\ K_{\Pi\Delta}^{(i)T} \end{array} \right] R_\Pi^{(i)}.$$

In section 6, we will present several choices of primal constraints and their implementation using a proper change of basis will be discussed in section 7. These choices are motivated by the requirements of our theoretical analysis that the elements in the range of an average operator should have a divergence-free extension into the subdomains and that the algorithm should perform well for compressible elasticity problems. One experimentally successful recipe involves using primal vertex constraints for all subdomain vertices, augmenting them with a primal constraint on the average of the normal displacement component over each subdomain face and the averages, over the subdomain edges, of the two displacement components orthogonal to each edge. This set of primal constraints does not fully meet the requirement of existing theory. The set of primal constraints also has to be enriched by additional edge averages and, for certain sets of Lamé parameters $\{\mu_i\}$, first order moments to enable us to give a full theoretical justification.

5. Convergence rate estimates. We now prove a bound on the BDDC convergence rate given a sufficiently rich sets of primal constraints as just outlined. More details on the choice of primal constraints will be provided in the next section. We make the following two assumptions concerning the operator $E_D = \widetilde{R}_\Gamma \widetilde{R}_{D,\Gamma}^T$ that returns a weighted average of the interface displacements across the interface Γ.

Assumption 1. The primal constraints are chosen such that E_D satisfies the no net flux condition

$$\int_{\partial\Omega_i} (\overline{R}_\Gamma(E_D\mathbf{u}_\Gamma)) \cdot \mathbf{n}_i dA = 0 \quad \forall \mathbf{u}_\Gamma \in \boldsymbol{V}_\Delta$$

for all subdomains. Here, $\overline{R}_\Gamma$, defined in (3.1), maps $\widetilde{\boldsymbol{V}}_\Gamma$ into the product space $\boldsymbol{V}_\Gamma$ and $\mathbf{n}_i$ is the unit outward normal of $\partial\Omega_i$.

Assumption 2. There exists a positive constant C, which is independent of n, H, h, N and the values of the Lamé parameters, such that

$$|\overline{R}_\Gamma(E_D\mathbf{u}_\Gamma)|_{E(\Gamma)} \leq C \left(1 + \log\left(n^2\frac{H}{h}\right)\right) |\overline{R}_\Gamma \mathbf{u}_\Gamma|_{E(\Gamma)} \quad \forall \mathbf{u}_\Gamma \in \widetilde{\boldsymbol{V}}_\Gamma,$$

where the $|\cdot|_{E(\Gamma)}$ - seminorm has been defined in (3.10).

We note that Assumption 2 essentially means that the BDDC algorithm converges well for problems of compressible elasticity. We next turn to our main result.

THEOREM 5.1. *Let Assumptions* 1 *and* 2 *hold. Then the BDDC preconditioned operator* $M^{-1}\widehat{S}_\Gamma$ *and the associated FETI-DP operator, using the same set of primal variables, have condition numbers bounded by*

$$\kappa_2(M^{-1}\widehat{S}_\Gamma) \leq C \max_{i=1,\dots,N} 4\left(1 + \frac{3/2}{\mu_i/\lambda_i + \beta_{n,i}^2}\right)\left(1 + \log\left(n^2\frac{H}{h}\right)\right)^2.$$

Here C *is the constant of Assumption* 2 *and independent of* n, N, H, h *and the values of the Lamé parameters. The parameter* $\beta_{n,i}$ *is the inf-sup parameter of the mixed* $Q_n - Q_{n-2}$ *spectral element method and the subdomain* Ω_i.

Proof. We will use the $\widehat{S}_\Gamma$ inner product, associated with the $\widehat{S}_\Gamma$-norm (3.7), to prove the necessary bounds for the eigenvalues of the preconditioned operator $M^{-1}\widehat{S}_\Gamma$, namely, a lower bound

$$\langle \mathbf{u}_\Gamma, \mathbf{u}_\Gamma \rangle_{\widehat{S}_\Gamma} \leq \langle \mathbf{u}_\Gamma, M^{-1}\widehat{S}_\Gamma \mathbf{u}_\Gamma \rangle_{\widehat{S}_\Gamma}$$

and an upper bound

$$\langle \mathbf{u}_\Gamma, M^{-1}\widehat{S}_\Gamma \mathbf{u}_\Gamma \rangle_{\widehat{S}_\Gamma} \leq C \max_{i=1,\ldots,N} 4\left(1 + \frac{3/2}{\mu_i/\lambda_i + \beta_{n,i}^2}\right)\left(1 + \log\left(n^2 \frac{H}{h}\right)\right)^2 \langle \mathbf{u}_\Gamma, \mathbf{u}_\Gamma \rangle_{\widehat{S}_\Gamma}.$$

Lower bound. Since $\widetilde{R}_\Gamma^T \widetilde{R}_{D\Gamma} = \widetilde{R}_{D\Gamma}^T \widetilde{R}_\Gamma = I$, we have

$$\langle \mathbf{u}_\Gamma, \mathbf{u}_\Gamma \rangle_{\widehat{S}_\Gamma} = \mathbf{u}_\Gamma^T \widehat{S}_\Gamma \widetilde{R}_{D\Gamma}^T \widetilde{R}_\Gamma \mathbf{u}_\Gamma = \mathbf{u}_\Gamma^T \widehat{S}_\Gamma \widetilde{R}_{D\Gamma}^T \widetilde{S}_\Gamma^{-1} \widetilde{S}_\Gamma \widetilde{R}_\Gamma \mathbf{u}_\Gamma = \langle \mathbf{w}_\Gamma, \widetilde{R}_\Gamma \mathbf{u}_\Gamma \rangle_{\widetilde{S}_\Gamma},$$

where $\mathbf{w}_\Gamma^T := \mathbf{u}_\Gamma^T \widehat{S}_\Gamma \widetilde{R}_{D\Gamma}^T \widetilde{S}_\Gamma^{-1}$. By the Cauchy–Schwarz inequality, it then follows that

$$\langle \mathbf{u}_\Gamma, \mathbf{u}_\Gamma \rangle_{\widehat{S}_\Gamma} \leq \langle \mathbf{w}_\Gamma, \mathbf{w}_\Gamma \rangle_{\widetilde{S}_\Gamma}^{1/2} \langle \widetilde{R}_\Gamma \mathbf{u}_\Gamma, \widetilde{R}_\Gamma \mathbf{u}_\Gamma \rangle_{\widetilde{S}_\Gamma}^{1/2} = \langle \mathbf{w}_\Gamma, \mathbf{w}_\Gamma \rangle_{\widetilde{S}_\Gamma}^{1/2} \langle \mathbf{u}_\Gamma, \mathbf{u}_\Gamma \rangle_{\widehat{S}_\Gamma}^{1/2},$$

since $\widehat{S}_\Gamma = \widetilde{R}_\Gamma^T \widetilde{S}_\Gamma \widetilde{R}_\Gamma$. Therefore, by squaring and canceling a common factor,

$$(5.1) \quad \langle \mathbf{u}_\Gamma, \mathbf{u}_\Gamma \rangle_{\widehat{S}_\Gamma} \leq \langle \mathbf{w}_\Gamma, \mathbf{w}_\Gamma \rangle_{\widetilde{S}_\Gamma} = \mathbf{u}_\Gamma^T \widehat{S}_\Gamma \widetilde{R}_{D\Gamma}^T \widetilde{S}_\Gamma^{-1} \widetilde{R}_{D\Gamma} \widehat{S}_\Gamma \mathbf{u}_\Gamma = \langle \mathbf{u}_\Gamma, M^{-1}\widehat{S}_\Gamma \mathbf{u}_\Gamma \rangle_{\widehat{S}_\Gamma}.$$

Upper bound. If $\mathbf{u}_\Gamma \in \widetilde{\boldsymbol{V}}_\Gamma$, then $\widetilde{R}_{D\Gamma}^T \mathbf{u}_\Gamma \in \widehat{\boldsymbol{V}}_\Gamma$, and with $E_D \mathbf{u}_\Gamma = \widetilde{R}_\Gamma \widetilde{R}_{D\Gamma}^T \mathbf{u}_\Gamma$,

$$(5.2) \qquad \|E_D \mathbf{u}_\Gamma\|_{\widetilde{S}_\Gamma}^2 = |\overline{R}_\Gamma(E_D \mathbf{u}_\Gamma)|_{S_\Gamma}^2 = \sum_{i=1}^N |\overline{R}_\Gamma(E_D \mathbf{u}_\Gamma)|_{S_\Gamma^{(i)}}^2.$$

We now note that the operator E_D maps any continuous function, e.g., those of $\widehat{\boldsymbol{V}}_\Pi$, into itself. Therefore when bounding $E_D \mathbf{u}_\Gamma$, we can confine ourselves to elements of $\boldsymbol{V}_\Delta$. By Assumption 1, $\overline{R}_\Gamma(E_D \mathbf{u}_\Gamma)$ then has zero net flux across the subdomain boundaries, and we can apply the right inequality of Lemma 3.1 to each local term in the sum on the right to obtain

$$(5.3) \qquad |\overline{R}_\Gamma(E_D \mathbf{u}_\Gamma)|_{S_\Gamma^{(i)}}^2 \leq 4\left(1 + \frac{3/2}{\mu_i/\lambda_i + \beta_{n,i}^2}\right)\mu_i |\overline{R}_\Gamma(E_D \mathbf{u}_\Gamma)|_{E(\Gamma_i)}^2.$$

By summing over the subdomains and using (5.2) and (3.10), we find

$$(5.4) \qquad \|E_D \mathbf{u}_\Gamma\|_{\widetilde{S}_\Gamma}^2 \leq \max_i 4\left(1 + \frac{3/2}{\mu_i/\lambda_i + \beta_{n,i}^2}\right)|\overline{R}_\Gamma(E_D \mathbf{u}_\Gamma)|_{E(\Gamma)}^2.$$

By Assumption 2, we can bound the last factor on the right in terms of $|\overline{R}_\Gamma \mathbf{u}_\Gamma|_{E(\Gamma)}$ and then return to $\widetilde{S}_\Gamma$-norm by summing the left inequalities of Lemma 3.1 over the subdomains and by using (3.8). We obtain

$$(5.5) \qquad \|E_D \mathbf{u}_\Gamma\|_{\widetilde{S}_\Gamma}^2 \leq C \max_i 4\left(1 + \frac{3/2}{\mu_i/\lambda_i + \beta_{n,i}^2}\right)\left(1 + \log\left(n^2 \frac{H}{h}\right)\right)^2 \|\mathbf{u}_\Gamma\|_{\widetilde{S}_\Gamma}^2.$$

Given $\mathbf{u}_\Gamma \in \widehat{\boldsymbol{V}}_\Gamma$, we now use $\mathbf{w}_\Gamma := \widetilde{S}_\Gamma^{-1}\widetilde{R}_{D\Gamma}\widehat{S}_\Gamma \mathbf{u}_\Gamma$, as in the proof of the lower bound. Then $\widetilde{R}_{D\Gamma}^T \mathbf{w}_\Gamma = M^{-1}\widehat{S}_\Gamma \mathbf{u}_\Gamma$ and

$$\langle M^{-1}\widehat{S}_\Gamma \mathbf{u}_\Gamma, M^{-1}\widehat{S}_\Gamma \mathbf{u}_\Gamma \rangle_{\widehat{S}_\Gamma} = \langle \widetilde{R}_{D\Gamma}^T \mathbf{w}_\Gamma, \widetilde{R}_{D\Gamma}^T \mathbf{w}_\Gamma \rangle_{\widehat{S}_\Gamma}$$
$$= \langle \widetilde{R}_\Gamma \widetilde{R}_{D\Gamma}^T \mathbf{w}_\Gamma, \widetilde{R}_\Gamma \widetilde{R}_{D\Gamma}^T \mathbf{w}_\Gamma \rangle_{\widetilde{S}_\Gamma} = \|E_D \mathbf{w}_\Gamma\|_{\widetilde{S}_\Gamma}^2$$

because $\widehat{S}_\Gamma = \widetilde{R}_\Gamma^T \widetilde{S}_\Gamma \widetilde{R}_\Gamma$ and the definition of E_D. From (5.5), it follows that

$$\|E_D \mathbf{w}_\Gamma\|_{\widetilde{S}_\Gamma}^2 \leq C \max_{i=1,\ldots,N} 4 \left(1 + \frac{3/2}{\mu_i/\lambda_i + \beta_{n,i}^2} \right) \left(1 + \log \left(n^2 \frac{H}{h} \right) \right)^2 \|\mathbf{w}_\Gamma\|_{\widetilde{S}_\Gamma}^2.$$

Since by (5.1), $\|\mathbf{w}_\Gamma\|_{\widehat{S}_\Gamma}^2 = \langle \mathbf{u}_\Gamma, M^{-1}\widehat{S}_\Gamma \mathbf{u}_\Gamma \rangle_{\widehat{S}_\Gamma}$, we have

$$\langle M^{-1}\widehat{S}_\Gamma \mathbf{u}_\Gamma, M^{-1}\widehat{S}_\Gamma \mathbf{u}_\Gamma \rangle_{\widehat{S}_\Gamma}$$

$$(5.6) \quad \leq C \max_{i=1,\ldots,N} 4 \left(1 + \frac{3/2}{\mu_i/\lambda_i + \beta_{n,i}^2} \right) \left(1 + \log \left(n^2 \frac{H}{h} \right) \right)^2 \langle \mathbf{u}_\Gamma, M^{-1}\widehat{S}_\Gamma \mathbf{u}_\Gamma \rangle_{\widehat{S}_\Gamma}.$$

From the Cauchy–Schwarz inequality and (5.6), we then have

$$\langle \mathbf{u}_\Gamma, M^{-1}\widehat{S}_\Gamma \mathbf{u}_\Gamma \rangle_{\widehat{S}_\Gamma}^2 \leq \langle \mathbf{u}_\Gamma, \mathbf{u}_\Gamma \rangle_{\widehat{S}_\Gamma} \langle M^{-1}\widehat{S}_\Gamma \mathbf{u}_\Gamma, M^{-1}\widehat{S}_\Gamma \mathbf{u}_\Gamma \rangle_{\widehat{S}_\Gamma}$$

$$\leq C \max_{i=1,\ldots,N} 4 \left(1 + \frac{3/2}{\mu_i/\lambda_i + \beta_{n,i}^2} \right) \left(1 + \log \left(n^2 \frac{H}{h} \right) \right)^2 \langle \mathbf{u}_\Gamma, \mathbf{u}_\Gamma \rangle_{\widehat{S}_\Gamma} \langle \mathbf{u}_\Gamma, M^{-1}\widehat{S}_\Gamma \mathbf{u}_\Gamma \rangle_{\widehat{S}_\Gamma},$$

and the upper bound follows by canceling a common factor. $\square$

6. Choice of primal constraints and Assumptions 1 and 2. We will now show how Assumptions 1 and 2 can be satisfied with a proper choice of primal constraints. We will consider the following subsets of primal variables:

- V, the displacements at the subdomain vertices;
- E_a^2, the averages of the normal displacements over each subdomain edge (2 averages per edge);
- E_a^3, the averages of the displacements over each subdomain edge (3 averages per edge, 1 per displacement component);
- E_m^2, the first order moments of the normal displacements over each subdomain edge (2 moments per edge);
- F_a^1, the average of the normal displacements over the interior of each subdomain face (1 average per face);
- F_a^3, the averages of the displacements over each subdomain face (3 averages per face, 1 per displacement component).

Our discussion will be based on the results of [36], as far as Assumption 1 is concerned, and on [33] for Assumption 2. As in all two-level domain decomposition algorithms, we have to observe the *null space* condition. The null space of the elasticity operator in three dimensions is spanned by the six rigid body motions, which are vector-valued functions with components which are linear functions; see, e.g., [33, section 2].

The averages, which define our primal constraints, can be viewed in terms of weights given by the restrictions of the rigid body motions to edges and faces. We note that for a straight edge, we can use no more than five primal constraints since the restrictions to an edge of the six rigid body modes are linearly dependent; see [33, pages 1540 and 1560].

We will use an additive notation to denote the union of sets of constraints. While in our theory, we need to include at least $V + E_a^3 + E_m^2 + F_a^1$, the numerical results

of section 8 indicate that in many cases, we obtain good convergence rates also with the smaller set of primal constraints $V + E_a^2 + F_a^1$. That latter choice is perfect for Assumption 1.

LEMMA 6.1. *Assumption* 1 *holds when the set of primal constraints contains the set* $V + E_a^2 + F_a^1$.

Proof. We need to show that $\int_{\partial\Omega_i} \mathbf{v}^{(i)} \cdot \mathbf{n}_i = 0$, where $\mathbf{v}^{(i)}$ is the component of $\overline{R}_\Gamma E_D \mathbf{u}_\Gamma$ associated with Ω_i and $\mathbf{u}_\Gamma \in \mathbf{V}_\Delta$. We consider each face F^{ij}, shared by Ω_i and Ω_j, of $\partial\Omega_i$ separately. Since the subdomain vertices are primal, we can decompose the integral over F^{ij} into face and edge components

$$(6.1) \qquad \int_{F^{ij}} \mathbf{v}^{(i)} \cdot \mathbf{n}_{ij} = \int_{F^{ij}} I^{n,h}(\theta_{F^{ij}} \mathbf{v}^{(i)}) \cdot \mathbf{n}_{ij} + \sum_{E^k \subset \partial F^{ij}} \int_{F^{ij}} I^{n,h}(\theta_{E^k} \mathbf{v}^{(i)}) \cdot \mathbf{n}_{ij},$$

where $I^{n,h}$ is the interpolation operator onto the spectral element space and $\theta_{F^{ij}}$ and θ_{E^k} are the standard partition-of-unity functions with the value 1 at the nodes on the face F^{ij} and the edge E^k, respectively, and which vanish at all other interface nodes. Since each element is a nondegenerate affine image of the reference cube, our mapped elements are polytopes with faces that are parallelograms and, in particular, with parallel mesh lines on the faces.

By using GLL quadrature, the first, the face term of (6.1), reduces to a sum over the GLL nodes interior to F^{ij}. Our choice of the primal constraints includes face averages of the normal displacements and after a change of basis, described in the next section, these averages will all vanish. Therefore the first term on the right-hand side of (6.1) will vanish.

Since the edge function $w_E = I^{n,h}(\theta_{E^k} \mathbf{u}_\Delta^{(i)}) \cdot \mathbf{n}_{ij}$ vanishes at all the GLL nodes on the interface, except at the nodes on E^k, we find, by using GLL quadrature over F^{ij} and with E^k located at $x = \xi_0$, that

$$\int_{F^{ij}} w_E ds = \sum_{i_1=0}^{n+1} \sum_{i_2=0}^{n+1} \sigma_{i_1} \sigma_{i_2} w_E(\xi_{i_1}, \xi_{i_2}) = \sigma_0 \sum_{i_2=0}^{n+1} \sigma_{i_2} w_E(\xi_0, \xi_{i_2}) = \sigma_0 \int_{E^k} w_E d\xi.$$

These edge averages all vanish after the change of basis of the next section and so do all the integrals of (6.1). □

LEMMA 6.2. *Assumption* 2 *holds when the set of primal constraints is acceptable in the sense of* [33, Definition 5.8]. *This is guaranteed, for any selection of the Lamé parameters* μ_i, *by using the primal set* $V + E_a^3 + E_m^2 + F_a^1$.

Proof. In the recipe developed in [33, section 5], *fully primal* faces and edges play an important role. A fully primal face is associated with at least six primal constraints, which provide a full six-dimensional dual basis for the space of rigid body motions. They cannot be based on vertex constraints since there is an additional requirement that all the functionals can be bounded by a logarithmic factor in the dimension of the local problems; vertex constraints are associated with operators which have norms which, in our context, would be linear in $n^2 H/h$.

It is shown in [35, section 7] that a third tangential edge constraint, as in E_a^3, will be required for at least one edge of a face of the interface to make it fully primal. This makes it necessary to use at least a substantial subset of the tangential edge averages of E_a^3 in our set of primal constraints. Should no tangential edge constraints be included, then all faces of the interface would fail to be primal. We note that an examination of the theory shows that, to assure success, there must exist relatively many fully primal faces in all parts of the domain.

The requirement that the set of primal constraints be acceptable will also at times make it necessary to make some edges of the interface fully primal; all edges will be fully primal by including $E_a^3 + E_m^2$ in the set of primal constraints. Such a set of five constraints for an individual edge can be needed in developing our bounds if the coefficients of the subdomains that have the edge in common have Lamé parameters μ_i that differ by orders of magnitude. An example can be given, in the case of four such subdomains, by selecting two very different values of μ_i in an alternating pattern when we move around the edge. Without patterns of such a nature, constraints based on the first order moment over edges are not required to establish strong bounds as in Theorem 5.1.

A full proof of the bound of Assumption 2 also requires the extension to the spectral element case of the finite element bound given in Klawonn and Widlund [33, Condition 8.1]. We note that the P_D operator of that work and E_D of the BDDC algorithm are complementary projectors with $E_D + P_D = I$. The modifications necessary are routine since the extension of the technical tools necessary from the finite element to the spectral element case can be carried out essentially as in Toselli and Widlund [48, subsection 7.4.1]. There these tools are presented in the special case of subdomains with one single element ($H/h = 1$). However, they can be easily extended to multielement subdomains by using the same technique of refining the GLL mesh inside each spectral element into a quasi-uniform mesh with mesh size equal to the smallest distance between GLL points, i.e., $O(1/n^2)$ on the reference element. The number of refined mesh points along a subdomain edge then becomes $O(n^2 H/h)$, and we can obtain counterparts of [48, Lemmas 7.11–7.15] with factors $1 + \log(n^2 H/h)$ instead of $1 + \log(n)$. We finally note that the auxiliary results Lemmas 7.1–7.5 of [33, section 7], which also involves first order moments, pose no new challenges. $\square$

We note that in the previous work on compressible elasticity, as in [33], the use of vertex constraints is avoided. By themselves, they do not allow for bounds of the same quality as in Theorem 5.1; see [34, 31, Algorithm A]. Here the situation is different since we use the vertex constraints in establishing Assumption 1. It is clear from our experiments, reported in section 8, that combining the primal constraints of $E_a^2 + F_a^1$ with the vertex set V often results in a performance which is virtually identical with that of the richer set $V + E_a^3 + F_a^1$. We note that a bound for the former case, which is considerably much worse than that of our main result, can be established by relying on a bound for the compressible case with primal vertex constraints only; see, in addition to the two papers cited above, [30, Theorem 6.3].

7. Implementation of primal constraints by a change of basis. We now describe the implementation of the edge and face constraints defined above by using a linear change of basis for each scalar component of the displacements. This change of basis will explicitly introduce the new primal degrees of freedom in the basis (for additional details see [37, 33, 28, 29]). We first consider the case of edge and face averages and then that of averages and first order moment constraints over the edges in the case of one element per subdomain, assumed for simplicity to be the reference element. A generalization to the case of more elements per subdomain is straightforward. We denote by $T^{(i)}$ the local transformation matrix, associated with Ω_i, from the new basis (denoted with a hat) to the original one,

$$u = T^{(i)}\hat{u}.$$

The local stiffness matrix in the new basis is then

(7.1) $$\widehat{K}^{(i)} := T^{(i)T} K^{(i)} T^{(i)}.$$

Such $T^{(i)}$ can be constructed by grouping together the contributions of each scalar edge and face components, together with an identity matrix for the interior component; see [37]. The new local stiffness matrices are denser than the original ones, but only the blocks related to the interface nodes are affected by the transformation, which indeed preserves the sparsity pattern for the interior nodes of the subdomain, since $\widehat{K}_{II}^{(i)} = K_{II}^{(i)}$. We will assume that such a transformation of basis has been performed before the construction of the preconditioner.

We note that the transformation of basis impacts the sparsity pattern much less than the elimination of the pressure variables. For example, we considered a discretization with $5 \times 3 \times 2$ spectral elements of degree $n = 3$ and found that the number of nonzero entries increased from about $1.24 \cdot 10^5$ to $8.85 \cdot 10^5$ (about a factor 7.14) when the pressures were eliminated, while the change of variable further increased the number of nonzero entries from $8.85 \cdot 10^5$ to $1.08 \cdot 10^6$ (by only a factor 1.22).

Edge averages. Consider a scalar component on an element edge E: it contains $n - 1$ GLL nodes since the endpoints are always associated with primal variables and are therefore not included in the dual part of the edge. In [37], the edge average change of basis is performed by splitting the dual part of each scalar component of the edge into the sum of two functions, a constant average function and another with a zero average,

$$
(7.2) \qquad \hat{u}_n \begin{pmatrix} 1 \\ \vdots \\ 1 \end{pmatrix} + \begin{pmatrix} \hat{u}_2 \\ \vdots \\ \hat{u}_{n-1} \\ -\sum_{i=2}^{n-1} \hat{u}_i \end{pmatrix}.
$$

$\hat{u}_n$ can then be selected as a primal degree of freedom associated with the edge average of the scalar component. In order to get the correct average in our GLL case, the change of basis over the edge is performed by using the matrix

$$
(7.3) \qquad T_E = \begin{bmatrix} 1 & 0 & \dots & 0 & 1 \\ & \ddots & & & \vdots \\ & & 1 & & 1 \\ & & & \ddots & \vdots \\ -\dfrac{\sigma_2}{\sigma_n} & \dots & \dots & -\dfrac{\sigma_{n-1}}{\sigma_n} & 1 \end{bmatrix},
$$

where σ_i are the weights of the one-dimensional GLL quadrature formula.

Face averages. Analogous transformation matrices T_F can be defined for the face constraints. As for the edges, the last element of the dual part of each scalar component on a face can be chosen as primal, and face averages can be obtained with the two-dimensional GLL quadrature rule based on tensor product. The transformation matrix obtained is then structurally similar to (7.3): the elements on the main diagonal and in the last column equal to 1, while the other matrix elements vanish except those of the last row, which are associated with the new primal degrees of freedom, and are given by

$$
(7.4) \qquad \left(-\dfrac{\sigma_2^2}{\sigma_n^2} \ \dots \ -\dfrac{\sigma_2 \sigma_{n-1}}{\sigma_n^2} \ \dots \ -\dfrac{\sigma_{n-1} \sigma_2}{\sigma_n^2} \ \dots \ -\dfrac{\sigma_{n-1}^2}{\sigma_n^2} \ 1 \right).
$$

Edge averages and first order moments. In a similar way, writing the transformation matrix by columns into

$$(7.5) \qquad [t_2 | \ldots | t_n],$$

we perform the change of basis by setting the first $n - 3$ columns to

$$t_j = (0, \ldots, 0, 1, \alpha_j, \beta_j, 0, \ldots, 0)^T,$$

with the value 1 in the $(j-1)$th position and α_j, β_j chosen such that t_j has zero average and first moment over the edge. These conditions imply that α_j, β_j solve the linear system

$$(7.6) \qquad \begin{cases} \sigma_j + \alpha_j \sigma_{j+1} + \beta_j \sigma_{j+2} = 0, \\ \xi_j \sigma_j + \xi_{j+1} \alpha_j \sigma_{j+1} + \xi_{j+2} \beta_j \sigma_{j+2} = 0 \end{cases}$$

for $2 \leq j \leq n - 2$ and where ξ_j are the GLL nodes, yielding

$$(7.7) \qquad \alpha_j = -\frac{\sigma_j}{\sigma_{j+1}} \frac{\xi_{j+2} - \xi_j}{\xi_{j+2} - \xi_{j+1}}, \quad \beta_j = \frac{\sigma_j}{\sigma_{j+2}} \frac{\xi_{j+1} - \xi_j}{\xi_{j+2} - \xi_{j+1}}.$$

The last two columns of the transformation matrix are obtained by making t_{n-1} a constant and equal to 1, while t_n is a linear function with values -1 and 1 at the edge endpoints and are evaluated at the GLL nodes of the edge.

8. Numerical results. We report in this section the results of parallel numerical experiments for the positive definite reformulation of the mixed elasticity system on Ω, a parallelepiped with homogeneous Dirichlet boundary conditions on one face and homogeneous Neumann boundary conditions on the remainder of the boundary. This system is discretized with GLL spectral elements, and the domain Ω is subdivided into $N = N_x \times N_y \times N_z$ cubic spectral elements, assembled into subdomains Ω_i with $(H/h)^3$ spectral elements each. The reduced interface system with the Schur complement matrix (3.4) is solved by the PCG algorithm with the BDDC preconditioner (4.1), a zero initial guess, and the stopping criterion $\|r_k\|_2 / \|r_0\|_2 \leq 10^{-6}$, where r_k is the residual of the kth iterate. The right-hand side is random and uniformly distributed.

Our code has been implemented in FORTRAN and run on both the small Linux cluster Ulisse (84 cores) of the University of Milan and the larger IBM SP6/5376 (5376 computing cores subdivided into 168 nodes) of CINECA (www.cineca.it). In order to assure parallelization and portability of the code, message passing has been implemented in message passing interface (MPI), while local data structures such as matrices and vectors are managed through the use of the portable, extensible toolkit for scientific computation (PETSc) library [3, 2]. Each subdomain is assigned to one core (here one MPI process); the local problems involved in Schur matrix-vector products and in the application of the BDDC local solvers are solved by the multifrontal method unsymmetric multifrontal package (UMFPACK) [10], whereas the BDDC coarse problem is solved by either the multifrontal solver multifrontal massively parallel sparse direct solver (MUMPS) [1] or by PCG run to almost machine precision (with relative tolerance 10^{-14}).

Effects of the choice of primal constraints. Table 8.1 reports the BDDC iteration counts (it), condition number (κ_2), which is essentially $\lambda_{\max}$ since $\lambda_{\min}$ is very close to 1, and CPU times (cpu) in seconds with different choices of primal constraints, ranging from just the subdomain vertices (V) to vertices augmented with edge and face

TABLE 8.1

BDDC iteration counts (it), condition numbers (κ_2) and CPU times (cpu) in seconds with different choices of primal constraints. Compressible material with $\nu = 0.4$ (left), almost incompressible material with $\nu = 0.49999$ (center), heterogeneous material with discontinuous Lamé parameters (right) given as in Figure 8.1. Fixed polynomial degree $n = 5$, number of subdomains (processors) $N = 3 \times 3 \times 3$, and $2 \times 2 \times 2$ elements per subdomain ($H/h = 2$).

Primal	$\nu = 0.4$			$\nu = 0.49999$			Random mix		
variables (# dofs)	it	κ_2	cpu	it	κ_2	cpu	it	κ_2	cpu
V (132)	94	250.65	10.6	112	5.3e+5	12.7	114	4.1e+7	13.5
$V+E_a^2$ (324)	22	9.69	2.6	23	2.3e+4	2.8	33	2.0e+6	4.0
$V+E_a^3$ (420)	19	7.98	2.4	21	2.1e+4	2.6	23	1.7e+6	2.8
$V+E_a^2+E_m^2$ (516)	19	7.17	2.3	23	2.2e+4	2.7	23	1.9e+6	2.8
$V+E_a^2+F_a^1$ (378)	22	9.48	2.8	23	10.0	2.9	32	27.13	4.0
$V+E_a^3+F_a^1$ (474)	19	7.79	2.5	21	9.19	2.7	24	12.03	3.0
$V+E_a^3+F_a^3$ (582)	19	7.71	2.5	21	9.11	2.8	24	11.06	3.1
$V+E_a^3+E_m^2+F_a^1$ (666)	14	4.10	1.8	16	5.69	2.1	20	7.37	2.6

λ				μ		
0.1	10^6	18		18	2.3	33
4	72	10^6		3.7	0.2	0.4
10^6	2.5	3		0.25	0.4	10

40	0.1	33		21	1	$3 \cdot 10^{-2}$
0.87	10^6	30		2.2	0.01	12
10	10^6	20		0.55	15	1

10^6	20	200		0.1	0.3	18
200	5	10^6		3.7	34	20
1	10^6	10		1	4	20
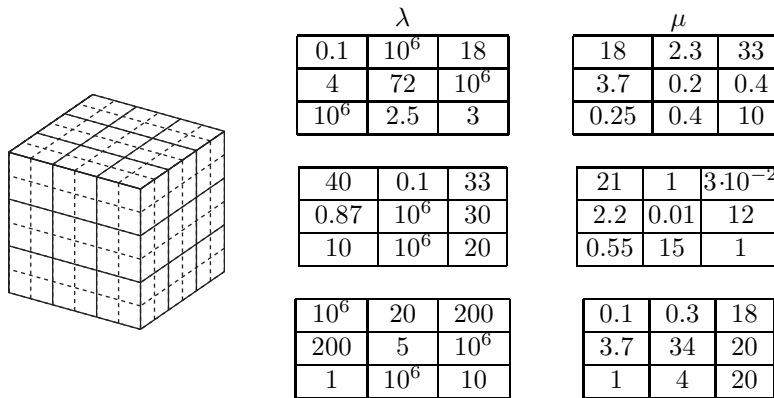
FIG. 8.1. *Domain Ω for the tests of Table 8.1 decomposed into $N = 3 \times 3 \times 3$ subdomains with $2 \times 2 \times 2$ elements per subdomain ($H/h = 2$) (left). Distribution on each 3×3 subdomain layer of the discontinuous Lamé parameters λ and μ for the "random mix" test of Table 8.1 (last column) (center and right).*

averages and edge first order moments ($V + E_a^3 + E_m^2 + F_a^1$). These results are reported for both compressible ($\nu = 0.4$) and almost incompressible ($\nu = 0.49999$) materials for tests with fixed polynomial degree $n = 5$, number of subdomains (processors) $N = 3 \times 3 \times 3$, and $2 \times 2 \times 2$ elements per subdomain ($H/h = 2$). The results show that the strength of the BDDC preconditioner increases when the set of primal constraints increases, with the minimal vertex choice performing quite poorly even in the easier compressible case. When the material becomes almost incompressible, all choices of primal constraints including only vertex and edge constraints lead to ill-conditioned BDDC operators (with κ_2 on the order of $10^4 - 10^5$). The BDDC operator becomes robust in the almost incompressible limit when at least the face average constraint for the normal displacement component (F_a^1) is added to the vertex and edge constraints, reducing κ_2 to about 10 or less.

The iteration counts, on the other hand, indicate a poor performance with vertex constraints only, while the inclusion of edge constraints seems to improve the iteration counts considerably. However, this is a misleading effect due to our stopping criterion, which is based on the relative residual: changing primal constraints changes the initial

TABLE 8.2

BDDC dependence on the polynomial degree n: iteration counts (it) and condition numbers (κ_2) with the first two choices of primal constraints that are robust in the incompressible limit, $V + E_a^2 + F_a^1$ and $V + E_a^3 + F_a^1$. Compressible material with $\nu = 0.4$ (left) and almost incompressible material with $\nu = 0.49999$ (right). Fixed number of subdomains (processors) $N = 3 \times 3 \times 3$, one element per subdomain ($H/h = 1$).

| | $\nu = 0.4$ | | | | $\nu = 0.49999$ | | | |
| | $V + E_a^2 + F_a^1$ | | $V + E_a^3 + F_a^1$ | | $V + E_a^2 + F_a^1$ | | $V + E_a^3 + F_a^1$ | |
n	it	κ_2	it	κ_2	it	κ_2	it	κ_2
2	7	1.66	5	1.27	7	1.66	5	1.26
3	10	2.64	9	2.12	13	3.85	11	3.84
4	14	4.57	12	3.66	15	4.91	15	4.91
5	17	5.65	14	4.87	18	6.80	17	6.80
6	19	7.71	17	6.41	20	8.32	19	7.65
7	21	8.60	18	7.30	22	9.41	22	9.08
8	23	10.54	20	8.69	24	11.60	23	10.84
9	24	11.40	21	9.48	26	12.61	25	12.17
10	26	13.17	22	10.75	28	14.68	26	13.79
11	28	13.99	24	11.47	30	15.69	28	15.06
12	29	15.62	25	12.61	31	17.59	29	16.56

residual; hence it changes the relative residual and the iteration counts. We have also computed the infinity norm of the error in each run (not reported), and we have found that indeed these errors are small only for the robust BDDC methods that also include at least the normal face constraints. The CPU times reported for each of the three tests (compressible, almost incompressible, random mix) are clearly proportional to the iteration counts, since they include only the solution time and not the preprocessing stage for the local and coarse problems. The last column of Table 8.1 reports analogous results for a harder test (random mix) with discontinuous Lamé parameters λ and μ distributed randomly among the subdomains as shown in Figure 8.1. Note that in this test several almost incompressible subdomains (with large λ/μ ratio) are mixed randomly with compressible subdomains, and different pairs of almost incompressible subdomains can share a whole face or an edge or a vertex. The results show that also in this test the BDDC preconditioned operator becomes well conditioned only if at least the face average constraint for the normal displacement component is added to the vertex and edge constraints, i.e., if at least $V + E_a^2 + F_a^1$ is included in the set of primal constraints.

Dependence on polynomial degree n. Table 8.2 reports the BDDC iteration counts and condition numbers for increasing polynomial degree n from 2 to 12, for both compressible and almost incompressible materials, and for the first two choices of primal constraints that are robust in the incompressible limit, namely, $V + E_a^2 + F_a^1$ and $V + E_a^3 + F_a^1$; we obtained almost the same results also for $V + E_a^3 + F_a^3$, which are not reported. In order to check the dependence of κ_2 on n, we show in Figure 8.2 the semilogx plots of $\sqrt{\kappa_2}$, using values from Table 8.2, as a function of n.

In spite of the alternating behavior associated with even and odd values of n, the results seem to confirm the $\log^2(n)$ upper bound of Theorem 5.1 (plotted here with dashed lines), since the semilogx plots well approximate straight lines when we disregard the first 2–3 points, i.e., those for $n \leq 3$. The values for the smaller set of primal constraints $V + E_a^2 + F_a^1$ are more irregular in the compressible case, where they seem to grow slightly faster than the values for $V + E_a^3 + F_a^1$. The slopes of the approximating straight lines in the compressible case are 1.48 for $V + E_a^3 + F_a^1$ and 1.65 for $V + E_a^2 + F_a^1$, while in the almost incompressible case the slopes are 1.67 for
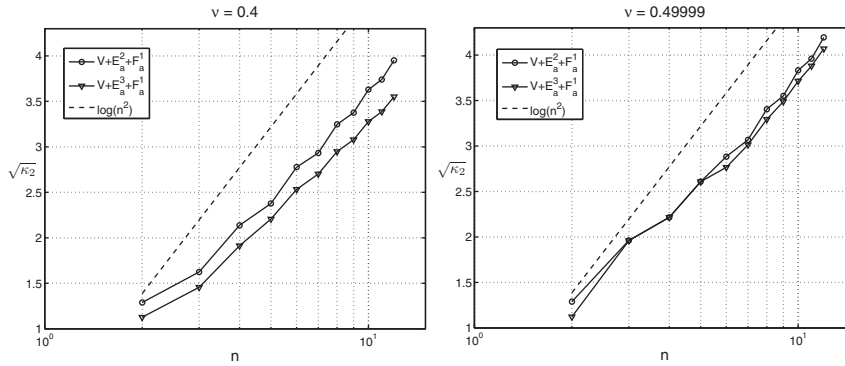
FIG. 8.2. *Square root of the BDDC condition number κ_2 as a function of n; data from Table 8.2. Compressible materials with $\nu = 0.4$ (left), almost incompressible materials with $\nu = 0.49999$ (right).*

TABLE 8.3

BDDC scalability: iteration counts (it) and condition numbers (κ_2) for an increasing number of subdomains (processors) N. Fixed $\nu = 0.49999$, polynomial degree $n = 3$, and $3 \times 3 \times 3$ elements per subdomain ($H/h = 3$). Number of global, interface, and primal dofs are also shown

N	$\dim(\mathbf{V}_n)$	$\dim(\widehat{\mathbf{V}}_\Gamma)$	$V + E_a^2 + F_a^1$			$V + E_a^3 + F_a^1$		
			$\dim(\widehat{\mathbf{V}}_\Pi)$	it	κ_2	$\dim(\widehat{\mathbf{V}}_\Pi)$	it	κ_2
2x2x2	19494	2970	106	17	7.16	132	15	5.33
4x4x2	75924	15336	472	20	7.27	592	17	6.10
6x6x2	169290	36990	1078	20	7.48	1356	18	6.27
8x8x2	299592	67932	1924	20	7.57	2424	18	6.33
10x10x2	466830	108162	3010	20	7.60	3796	18	6.36
12x12x2	671004	157680	4336	20	7.58	5472	18	6.39
14x14x2	912114	216486	5902	19	7.61	7452	17	6.39
16x16x2	1190160	284580	7708	19	7.57	9736	16	6.37

$V + E_a^3 + F_a^1$ and 1.8 for $V + E_a^2 + F_a^1$. These slopes of the n-semilogx plots are about twice the slopes of the analogous (H/h)-semilogx plots of Figure 8.4, (see comment below), in agreement with the bound of Theorem 5.1, where the log argument is quadratic in n and linear in H/h.

Scalability. Table 8.3 reports the BDDC iteration counts and condition numbers for increasing number of subdomains N, while keeping all the other parameters fixed ($n = 3, H/h = 3$) and considering only almost incompressible materials and the two primal spaces $V + E_a^2 + F_a^1$ and $V + E_a^3 + F_a^1$. The dimensions of the discrete global space $\mathbf{V}_n$, the interface space $\widehat{\mathbf{V}}_\Gamma$, and primal space $\widehat{\mathbf{V}}_\Pi$ are also reported, showing that the number of primal constraints, $dim(\widehat{\mathbf{V}}_\Pi)$, for the two primal spaces is a small percentage of that of $dim(\widehat{\mathbf{V}}_\Gamma)$. It decreases from 3.5% to 2.7% for increasing N for $V + E_a^2 + F_a^1$ and from 4.4% to 3.4% for $V + E_a^3 + F_a^1$. The condition numbers for both primal sets are then plotted in Figure 8.3 as a function of N. These results clearly show the scalability of the BDDC algorithm in the almost incompressible limit. As expected, the larger primal space $V + E_a^3 + F_a^1$ has a slightly better performance than $V + E_a^2 + F_a^1$.

Dependence on the ratio H/h. Table 8.4 reports the BDDC iteration counts and condition numbers for an increasing ratio H/h. We consider compressible materials with $\nu = 0.3$ (left), almost incompressible materials with $\nu = 0.49999$ (right), and the same robust choices of primal constraints of the previous tables, i.e., $V + E_a^2 + F_a^1$ and $V + E_a^3 + F_a^1$. Figure 8.4 shows the semilogx plots of $\sqrt{\kappa_2}$ from Table 8.4 as a
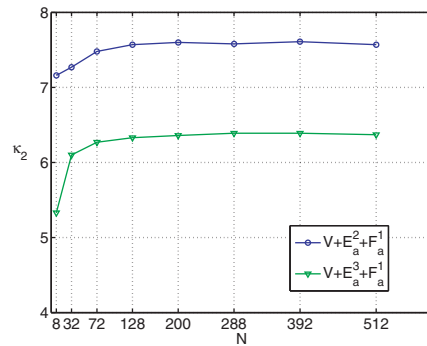
FIG. 8.3. *BDDC scalability: condition number κ_2 for increasing number of subdomains N; cf. Table 8.3.*

TABLE 8.4

BDDC dependence on H/h: iteration counts (it) and condition numbers (κ_2) for an increasing ratio H/h for the two choices of primal constraints $V + E_a^2 + F_a^1$ and $V + E_a^3 + F_a^1$. Compressible material with $\nu = 0.3$ (left) and almost incompressible material with $\nu = 0.49999$ (right). Polynomial degree $n = 3$, number of subdomains $N = 3 \times 3 \times 3$.

| | $\nu = 0.3$ | | | | $\nu = 0.49999$ | | | |
| | $V + E_a^2 + F_a^1$ | | $V + E_a^3 + F_a^1$ | | $V + E_a^2 + F_a^1$ | | $V + E_a^3 + F_a^1$ | |
H/h	it	κ_2	it	κ_2	it	κ_2	it	κ_2
1	10	2.64	8	2.10	13	3.86	11	3.84
2	16	5.20	13	4.07	16	5.26	14	4.28
3	19	7.16	16	5.51	19	7.16	17	6.16
4	21	8.77	17	6.65	21	8.76	19	7.56
5	23	10.15	18	7.61	23	10.12	20	8.76
6	24	11.36	19	8.43	25	11.32	22	9.79
7	26	12.45	21	9.17	26	12.39	22	10.69
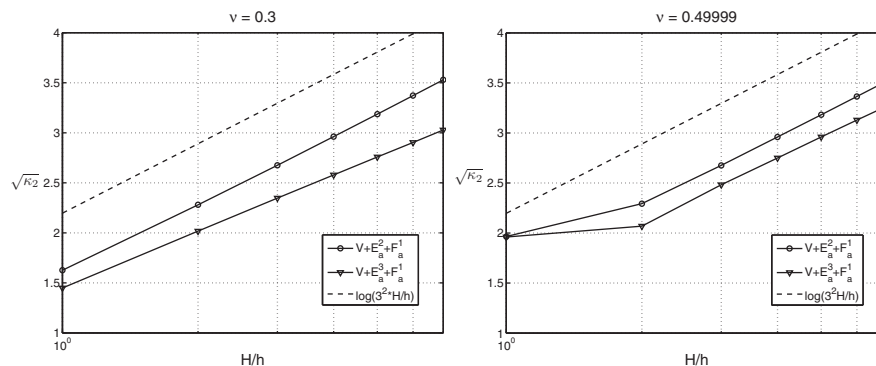
FIG. 8.4. *Square root of BDDC condition number κ_2 for increasing subdomain size H/h; cf. Table 8.4. Compressible materials with $\nu = 0.3$ (left), almost incompressible materials with $\nu = 0.49999$ (right).*

function of the ratio H/h. Here no odd-even oscillations are present since the spectral degree is fixed to $n = 3$; the plots appear to be straight lines (disregarding the first point in the almost incompressible case), with slope about 1.01 for $V + E_a^2 + F_a^1$ and 0.80 for $V + E_a^3 + F_a^1$ in the compressible case (left panel) and 0.99 and 0.93 in the almost incompressible case (right panel). These values give about half the slopes of
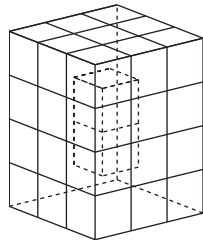
E_1/E_2	$V+E_a^2+F_a^1$		$V+E_a^3+F_a^1$		$V+E_a^3+E_m^2+F_a^1$	
	it	κ_2	it	κ_2	it	κ_2
10^{-6}	27	16.52	22	9.82	22	7.20
1	26	12.41	22	9.94	16	5.35
10^6	40	156.06	30	17.95	20	9.28

FIG. 8.5. *Jumping coefficients E and ν: BDDC iteration counts (it) and condition numbers (κ_2) with different choices of primal constraints. Domain with $N = 3 \times 3 \times 4$ subdomains (processors), each with $3 \times 3 \times 3$ elements ($H/h = 3$) with polynomial degree $n = 5$. Jumping Young modulus E and Poisson ratio ν, equal to $E = E_1$, $\nu = 0.49999$ in the two central subdomains sharing a face (see plot at left) and equal to $E = E_2 = 210$, $\nu = 0.3$ in the surrounding subdomains.*
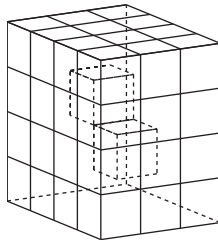
E_1/E_2	$V+E_a^2+F_a^1$		$V+E_a^3+F_a^1$		$V+E_a^3+E_m^2+F_a^1$	
	it	κ_2	it	κ_2	it	κ_2
10^{-6}	27	16.05	21	9.27	16	5.15
1	27	13.28	22	10.15	16	5.27
10^6	33	34.97	28	33.70	17	5.19

FIG. 8.6. *Jumping coefficients E and ν: BDDC iteration counts (it) and condition numbers (κ_2) with different choices of primal constraints. Domain with $N = 3 \times 4 \times 4$ subdomains (processors), each with $3 \times 3 \times 3$ elements ($H/h = 3$) with polynomial degree $n = 5$. Jumping Young modulus E and Poisson ratio ν, equal to $E = E_1$, $\nu = 0.49999$ in the two central subdomains sharing an edge (see plot at left) and equal to $E_2 = 210$, $\nu = 0.3$ in the surrounding subdomains.*

the analogous n-semilogx plots of Figure 8.2, in agreement with the $\log^2(n^2 \frac{H}{h})$ bound of Theorem 5.1. This agreement is also confirmed by comparing the plots with the dashed lines giving the upper bound predicted by the theory, which in this case with $n = 3$ states that $\sqrt{\kappa_2}$ should grow as $\log(3^2 H/h)$ (up to a constant and the local inf-sup contants).

Robustness with respect to discontinuities of material parameters. In addition to the test of Table 8.1, with a random mix of compressible and almost incompressible subdomains, we consider here two simpler tests with jumping coefficients E and ν, as in Figures 3 and 5 of [29]. First we consider a domain decomposed into $3 \times 3 \times 4$ subdomains as in Figure 8.5. All subdomains have Young modulus $E_2 = 210$ and Poisson ratio $\nu = 0.3$, except the two interior subdomains sharing a face that have $\nu = 0.49999$ and Young modulus E_1 varying by twelve orders of magnitude compared with E_2. The resulting BDDC iteration counts and condition numbers are reported in the table in Figure 8.5 for the three primal spaces $V + E_a^2 + F_a^1$, $V + E_a^3 + F_a^1$, and $V + E_a^3 + E_m^2 + F_a^1$ of increasing size and strength. In the second test of Figure 8.6 the situation is the same except that the two interior subdomains now share an edge instead of a face and that the domain consists of $3 \times 4 \times 4$ subdomains. In both tests, the harder case is when the surrounding subdomains have $E_1/E_2 = 10^6$, while in the reverse case $E_1/E_2 = 10^{-6}$ all primal sets have a performance very close to

that of the homogeneous case with $E_1/E_2 = 1$. We have obtained analogous results (not shown) in tests where only E has discontinuities and ν has constant value 0.3 or 0.49999. In Figure 8.5, $V + E_a^2 + F_a^1$ suffers the most when E_1/E_2 increases from 1 to 10^6, with κ_2 increasing by more of a factor 10 from about 12 to more than 150. $V + E_a^3 + F_a^1$ appears to be a bit more robust, but κ_2 still increases from about 9.9 to about 17.9. $V + E_a^3 + E_m^2 + F_a^1$ has the more robust performance, with $\kappa_2 \leq 9.3$. This situation is confirmed in Figure 8.6: both $V + E_a^2 + F_a^1$ and $V + E_a^3 + F_a^1$ suffer when E_1/E_2 increases from 1 to 10^6, with κ_2 increasing from about 10 to more than 33, while $V + E_a^3 + E_m^2 + F_a^1$ is robust in all cases, with $\kappa_2 \leq 5.3$. Indeed, only with the primal set $V + E_a^3 + E_m^2 + F_a^1$ is the edge fully primal. We also tried other combinations (e.g., reversing the jumps in ν between central and surrounding subdomain or with uncorrelated jumps of E and ν in different subdomains) and obtained results analogous to the ones reported in Figures 8.5 and 8.6. We remark that unlike [29], we also obtain good results in some cases where the edge is not fully primal; this may be due to the additional primal vertex constraints in our coarse space.

REFERENCES

[1] P. AMESTOY, ET AL., *MUMPS Web Page*, http://mumps.enseeiht.fr/.

[2] S. BALAY, K. BUSCHELMAN, V. EIJKHOUT, W. D. GROPP, D. KAUSHIK, M. G. KNEPLEY, L. C. MCINNES, B. F. SMITH, AND H. ZHANG, *PETSc Users Manual*, Revision 3.0, Technical report ANL-95/11 - Revision 3.0.0, Argonne National Laboratory, Chicago, 2008.

[3] S. BALAY, K. BUSCHELMAN, W. D. GROPP, D. KAUSHIK, M. G. KNEPLEY, L. C. MCINNES, B. F. SMITH, AND H. ZHANG, *PETSc Web Page*, http://www.mcs.anl.gov/petsc.

[4] L. BEIRÃO DA VEIGA, C. CHINOSI, C. LOVADINA, AND L. F. PAVARINO, *Robust BDDC preconditioners for Reissner–Mindlin plate bending problems and MITC elements*, SIAM J. Numer. Anal., 47 (2010), pp. 4214–4238.

[5] L. BEIRÃO DA VEIGA, C. LOVADINA, AND L. F. PAVARINO, *Positive definite balancing Neumann-Neumann preconditioners for nearly incompressible elasticity*, Numer. Math., 104 (2006), pp. 271–296.

[6] C. BERNARDI AND Y. MADAY, *Uniform inf-sup conditions for the spectral discretization of the Stokes problem*, Math. Models Methods Appl. Sci., 9 (1999), pp. 395–414.

[7] S. C. BRENNER AND L.-Y. SUNG, *BDDC and FETI-DP without matrices or vectors*, Comput. Methods Appl. Mech. Engrg., 196 (2007), pp. 1429–1435.

[8] F. BREZZI AND M. FORTIN, *Mixed and Hybrid Finite Element Methods*, Springer, Berlin, 1991.

[9] C. CANUTO, M. Y. HUSSAINI, A. QUARTERONI, AND T. A. ZANG, *Spectral methods*, in Evolution to Complex Geometries and Applications to Fluid Dynamics, Sci. Comput., Springer, Berlin, 2007.

[10] T. A. DAVIS, *Algorithm 832: UMFPACK, an unsymmetric-pattern multifrontal method*, ACM Trans. Math. Software, 30 (2004), pp. 196–199.

[11] M. O. DEVILLE, P. F. FISCHER, AND E. H. MUND, *High-order methods for incompressible fluid flow*, Cambridge Monogr. Appl. Comput. Math. 9, Cambridge University Press, Cambridge, 2002.

[12] M. DOBROWOLSKI, *On the LBB constant on stretched domains*, Math. Nachr., 254–255 (2003), pp. 64–67.

[13] C. R. DOHRMANN, *A preconditioner for substructuring based on constrained energy minimization*, SIAM J. Sci. Comput., 25 (2003), pp. 246–258.

[14] C. R. DOHRMANN, *A Substructuring Preconditioner for Nearly Incompressible Elasticity Problems*, Technical report SAND2004-5393, Sandia National Laboratories, Albuquerque, NM, 2004.

[15] C. R. DOHRMANN, *An approximate BDDC preconditioner*, Numer. Linear Algebra Appl., 14 (2007), pp. 149–168.

[16] C. R. DOHRMANN AND O. B. WIDLUND, *Hybrid domain decomposition algorithms for compressible and almost incompressible elasticity*, Internat. J. Numer. Methods Engrg., 82 (2010), pp. 157–183.

[17] C. R. DOHRMANN AND O. B. WIDLUND, *An overlapping Schwarz algorithm for almost incompressible elasticity*, SIAM J. Numer. Anal., 47 (2009), pp. 2897–2923.

[18] M. DRYJA, J. GALVIS, AND M. SARKIS, *BDDC methods for discontinuous Galerkin discretization of elliptic problems*, J. Complexity, 23 (2007), pp. 715–739.

[19] C. FARHAT, M. LESOINNE, P. LETALLEC, K. PIERSON, AND D. RIXEN, *FETI-DP: A dual-primal unified FETI method – part* I. *A faster alternative to the two-level FETI method*, Internat. J. Numer. Methods Engrg., 50 (2001), pp. 1523–1544.

[20] J. GALVIS AND M. SARKIS, *BDD and FETI Methods for Mortar Coupling of Stokes-Darcy Systems*, Commun. Appl. Math. Comput. Sci., 5 (2010), pp. 1–30.

[21] L. GHEZZI, L. F. PAVARINO, AND E. ZAMPIERI, *Overlapping Schwarz preconditioners for spectral element methods in nonstandard domains and heterogeneous media*, J. Comput. Appl. Math. 234 (2010), pp. 1492–1504.

[22] P. GOLDFELD, L. F. PAVARINO, AND O. B. WIDLUND, *Balancing Neumann-Neumann preconditioners for mixed approximations of heterogeneous problems in linear elasticity*, Numer. Math., 95 (2003), pp. 283–324.

[23] H. H. KIM, *A BDDC algorithm for mortar discretization of elasticity problems*, SIAM J. Numer. Anal., 46 (2008), pp. 2090–2111.

[24] H. H. KIM, M. DRYJA, AND O. B. WIDLUND, *A BDDC method for mortar discretizations using a transformation of basis*, SIAM J. Numer. Anal., 47 (2008), pp. 136–157.

[25] H. H. KIM AND X. TU, *A three-level BDDC algorithm for mortar discretizations*, SIAM J. Numer. Anal., 47 (2009), pp. 1576–1600.

[26] A. KLAWONN AND L. F. PAVARINO, *Overlapping Schwarz methods for elasticity and Stokes problems*, Comput. Methods Appl. Mech. Engrg., 165 (1998), pp. 233–245.

[27] A. KLAWONN, L. F. PAVARINO, AND O. RHEINBACH, *Spectral element FETI-DP and BDDC preconditioners with multi-element subdomains*, Comput. Methods Appl. Mech. Engrg., 198 (2008), pp. 511–523.

[28] A. KLAWONN AND O. RHEINBACH, *A parallel implementation of dual-primal FETI methods for three-dimensional linear elasticity using a transformation of basis*, SIAM J. Sci. Comput. 28 (2006), pp. 1886–1906.

[29] A. KLAWONN AND O. RHEINBACH, *Robust FETI-DP methods for heterogeneous three dimensional elasticity problems*, Comput. Methods Appl. Mech. Engrg., 196 (2007), pp. 1400–1414.

[30] A. KLAWONN AND O. RHEINBACH, *Highly scalable parallel domain decomposition methods with an application to biomechanics*, Z. Angew. Math. Mech., 90 (2010), pp. 5–32.

[31] A. KLAWONN, O. RHEINBACH, AND O. WIDLUND, *Some computational results for dual-primal FETI methods for elliptic problems in* 3D, in Domain Decomposition Methods in Science and Engineering XV, Lect. Notes Comput. Sci. Eng. 40, Springer, Berlin, 2005, pp. 361–368.

[32] A. KLAWONN, O. RHEINBACH, AND B. WOHLMUTH, *Dual-primal iterative substructuring for almost incompressible elasticity*, in Domain Decomposition Methods in Science and Engineering XVI, Lect. Notes Comput. Sci. Eng. 55, Springer, Berlin, 2007, pp. 397–404.

[33] A. KLAWONN AND O. B. WIDLUND, *Dual-primal FETI methods for linear elasticity*, Comm. Pure Appl. Math., 59 (2006), pp. 1523–1572.

[34] A. KLAWONN, O. WIDLUND, AND M. DRYJA, *Dual–primal FETI methods for three-dimensional elliptic problems with heterogeneous coefficients*, SIAM J. Numer. Anal., 40 (2002), pp. 159–179.

[35] J. LI, *A dual-primal FETI method for incompressible Stokes equations*, Numer. Math., 102 (2005), pp. 257–275.

[36] J. LI AND O. B. WIDLUND, *BDDC algorithms for incompressible Stokes equations*, SIAM J. Numer. Anal., 44 (2006), pp. 2432–2455.

[37] J. LI AND O. B. WIDLUND, *FETI-DP, BDDC, and block Cholesky methods*, Internat. J. Numer. Methods Engrg., 66 (2006), pp. 250–271.

[38] J. LI AND O. B. WIDLUND, *On the use of inexact subdomain solvers for BDDC algorithms*, Comput. Methods Appl. Mech. Engrg., 196 (2007), pp. 1415–1428.

[39] J. LI AND X. TU, *Convergence analysis of a balancing domain decomposition method for solving a class of indefinite linear systems*, Numer. Linear Algebra Appl., 16 (2009), pp. 745–773.

[40] Y. MADAY, D. MEIRON, A. T. PATERA, AND E. M. RØNQUIST, *Analysis of iterative methods for the steady and unsteady Stokes problem: Application to spectral element discretizations*, SIAM J. Sci. Comput., 14 (1993), pp. 310–337.

[41] J. MANDEL, C. R. DOHRMANN, AND R. TEZAUR, *An algebraic theory for primal and dual substructuring methods by constraints*, Appl. Numer. Math., 54 (2005), pp. 167–193.

[42] J. MANDEL AND B. SOUSEDÍK, *BDDC and FETI-DP under minimalist assumptions*, Computing, 81 (2007), pp. 269–280.

[43] J. MANDEL, B. SOUSEDÍK, AND C. R. DOHRMANN, *Multispace and multilevel BDDC*, Computing, 83 (2008), pp. 55–85.

[44] L. F. PAVARINO, *BDDC and FETI-DP preconditioners for spectral element discretizations*, Comput. Methods Appl. Mech. Engrg., 196 (2007), pp. 1380–1388.

[45] L. F. PAVARINO AND O. B. WIDLUND, *Iterative substructuring methods for spectral element discretizations of elliptic systems.* II. *Mixed methods for linear elasticity and Stokes flow*, SIAM J. Numer. Anal., 37 (2000), pp. 375–402.

[46] L. F. PAVARINO AND O. B. WIDLUND, *Balancing Neumann-Neumann methods for incompressible Stokes equations*, Comm. Pure Appl. Math., 55 (2002), pp. 302–335.

[47] L. F. PAVARINO AND O. B. WIDLUND, *BDDC and FETI-DP preconditioners for spectral element discretizations of almost incompressible elasticity*, in Spectral and High Order Methods for Partial Differential Equations, J. S. Hesthaven and E. Ronquist, eds., Lecture Notes in Comput. Engrg. 76, 2009, pp. 479–486.

[48] A. TOSELLI AND O. B. WIDLUND, *Domain Decomposition Methods—Algorithms and Theory*, Springer, New York, 2005.

[49] X. TU, *A BDDC algorithm for flow in porous media with a hybrid finite element discretization*, Electron. Trans. Numer. Anal., 26 (2007), pp. 146–160.

[50] X. TU, *Three-level BDDC in three dimensions*, SIAM J. Sci. Comput., 29 (2007), pp. 1759–1780.

[51] X. TU AND J. LI, *A balancing domain decomposition method by constraints for advection-diffusion problems*, Commun. Appl. Math. Comput. Sci., 3 (2008), pp. 25–60.